PHYSICAL REVIEW E **71**, 015402(R) (2005)

Impurity and trace tritium transport in tokamak edge turbulence

V. Naulin
Association EURATOM-Risø National Laboratory, OPL-128 Risø, DK-4000 Roskilde, Denmark
(Received 26 March 2004; revised manuscript received 26 May 2004; published 20 January 2005)

The turbulent transport of impurity or minority species, as for example tritium, is investigated in drift-Alfvén edge turbulence. The full effects of perpendicular and parallel convection are kept for the impurity species. The impurity density develops a granular structure with steep gradients and locally exceeds its initial values due to the compressibility of the flow. An approximate decomposition of the impurity flux into a diffusive part and an effective convective part (characterized by a pinch velocity) is performed and a net inward pinch effect is recovered. The pinch velocity is explained in terms of turbulent equipartition [Nycander and Yan'kov, Phys. Plasmas **2**, 2874 (1995)] and is found to vary poloidally. An approximate relationship between pinch velocity and turbulent diffusion is suggested.

DOI: 10.1103/PhysRevE.71.015402 PACS number(s): 52.25.Gj, 52.35.Ra, 52.65.Kj

The transport properties of impurities are of great concern in magnetic fusion devices. In particular impurities accumulate in the center of the plasma, where they are responsible for significant radiation losses. It is well established that turbulence is the key drive for plasma transport in the edge region and turbulence will also dominate the transport of impurities in that region. While in neutral fluids the transport of passive scalars is a very active field of research [2], it has in the context of plasma turbulence not yet found corresponding attention and measurements of impurity transport are most often interpreted within reduced one-dimensional (1D) transport models [3,4]. In plasma turbulence the velocity fields are in general compressible, making transport and mixing more complex than in incompressible flows [2] and putting strong demands on the numerical modeling.

Pinching of impurities has been observed as well as fast inwards transport of trace tritium in JET tritium puffs [5]. Especially in the edge region an inward convective flux (pinch) of impurities is found, which is proportional to the measured diffusion [3]. In the core, where anomalous, turbulent transport is less important than in the edge, the observed inward pinch of impurities seems to be in good agreement with neoclassical predictions based on trapped particle orbits. The Pfirsch-Schlüter impurity transport in the edge [6], leads to an inward impurity pinch due to ion-impurity collisions. However, there is no explanation for the high inward pinch velocities needed to describe impurity transport through the turbulent edge region and its scaling with the effective diffusion.

We investigate the transport of impurities as a passive tracer field in electromagnetic edge turbulence described by a standard model of drift-Alfvén turbulence [7–9]. Flux tube geometry is used, with local slablike coordinates (x,y,s) [10], corresponding roughly to the local radial, toroidal, and parallel directions. Note that within flux tube geometry motion along magnetic-field lines covers the poloidal extend of the tokamak, as the field lines wind around the tokamak. The following equations for the fluctuations in density n, potential ϕ with associated vorticity $\omega=\nabla_\perp^2\phi$, current J, and parallel ion velocity u, arise in the usual drift scaling:

$$\frac{\partial\omega}{\partial t}+\{\phi,\omega\}=\mathcal{K}(n)+\nabla_\parallel J+\mu_\omega\nabla_\perp^2\omega, \tag{1a}$$

$$\frac{\partial n}{\partial t}+\{\phi,n_{EQ}+n\}=\mathcal{K}(n-\phi)+\nabla_\parallel(J-u)+\mu_n\nabla_\perp^2 n, \tag{1b}$$

$$\frac{\partial}{\partial t}(\hat{\beta}A_\parallel+\hat{\mu}J)+\hat{\mu}\{\phi,J\}=\nabla_\parallel(n_{EQ}+n-\phi)-CJ, \tag{1c}$$

$$\hat{\varepsilon}\left(\frac{\partial u}{\partial t}+\{\phi,u\}\right)=-\nabla_\parallel(n_{EQ}+n). \tag{1d}$$

In addition to cross-field advection, the parallel derivatives carry nonlinearities entering through $A_\parallel$. The operator $\mathcal{K}$ represents effects of normal and geodesic curvature due to magnetic-field inhomogeneity with $\omega_B=2(L_\perp/R)$, R being the tokamak major radius, and $L_\perp$ the mean gradient length of the pressure profile,

$$\nabla_\parallel n=\frac{\partial n}{\partial s}-\hat{\beta}\{A_\parallel,n\},\quad \mathcal{K}(n)=-\omega_B\left(\sin s\frac{\partial n}{\partial x}+\cos s\frac{\partial n}{\partial y}\right).$$

The parallel current J is connected to the magnetic potential by $J=-\nabla_\perp^2 A_\parallel$. The parameters reflect the competition between parallel and perpendicular dynamics, represented in the scale ratio $\hat{\varepsilon}=(qR/L_\perp)^2$, where q is the safety factor. The electron parallel dynamics is controlled by the parameters

$$\hat{\beta}=\frac{2\mu_0 p_{e,0}}{B^2}\hat{\varepsilon},\quad \hat{\mu}=\frac{m_e}{M_i}\hat{\varepsilon},\quad C=0.51\frac{L_\perp}{\tau_e c_s}\hat{\mu}=\nu\hat{\mu}, \tag{2}$$

with τ_e being the electron collision time and the factor 0.51 reflecting parallel resistivity [11]. n_{EQ} is an equilibrium density associated with corresponding neoclassical fields and currents. Geodesic curvature acting on the equilibrium density is balanced by the neoclassical Pfirsch-Schlüter current $\mathcal{K}(n_{EQ})=-\nabla_\parallel J_{PS}$, which in turn is driven by the corresponding neoclassical potential $J_{PS}=1/C\nabla_\parallel\phi_{PS}$.

We assume the contribution of impurities to the gross plasma density $n_{i,0}$ to be negligible, i.e., $n_i=n_{i,0}+n_{imp}\approx n_{i,0}$. In experiments the assumption $n_{i,0}\gg n_{imp}$ is possibly not always fulfilled, especially not during the initial phase of a gas puff, where locally the puffed gas might contribute a signifi-

cant part of overall plasma density. While the bulk plasma is quasineutral with $n_e = n_{i,0}$, allowing to regard either the ion or electron continuity equation to determine the evolution of the density fluctuations, a corresponding relation for n_{imp} cannot be used. For cold impurities the ion-drift velocity is given by the $E \times B$ and the polarization drift, and thus

$$d_t n_{imp} = \frac{M}{Z\hat{\varepsilon}} \nabla_\perp \cdot (n_{imp} d_t \nabla_\perp \phi) - n_{imp} \mathcal{K}(\phi) - \nabla_\parallel (n_{imp} u) - \mu_{imp} \nabla_\perp^2 n_{imp} \tag{3}$$

determines the evolution of the impurity density. Here we introduced the relative mass of the impurities $M = M_{imp}/M_i$ and Z indicates their charge state. The fluctuating quantities ϕ and u are input from the dynamical evolution of the turbulence and the total time derivative d_t includes advection with the compressible $E \times B$ velocity. Equation (3) differs from the dynamical equation for the density fluctuations, Eq. (1b), as it does not reflect properties of the equilibrium, and moreover, in the sense that simplifications originating from the distinction between background and fluctuations are not appropriate for the impurities. Therefore here, all convection terms need to be preserved, while, for example, parallel convection is neglected in the equation for the density fluctuations. Finally, finite inertia effects of the impurity ions enter through the ion-polarization drift, however, for the remainder of this paper we consider massless impurities.

Standard parameters for simulation runs were $\hat{\mu} = 5$, $q = 3$, magnetic shear $\hat{s} = 1$ (appearing only in the geometrical set up of the simulations [7]), and $\omega_B = 0.05$, with the viscosities set to $\mu_\omega = \mu_n = 0.025$, corresponding to typical edge parameters of large fusion devices. Simulations were performed on a grid with $128 \times 512 \times 32$ points and dimensions $64 \times 256 \times 2\pi$ in x, y, s corresponding to a typical approximate dimensional size of 2.5 $\times 10$ cm $\times 30$ m [7]. Here we present results from a low $\hat{\beta} = 0.1$ run with $\nu = 2.295$. In the saturated turbulent state the equilibrium density gradient is weakly flattened. Strong deviations from the initially specified density gradient are prevented by a feedback mechanism using damping layers at the inner and outer radial boundary. This forces the density gradient to stay close to its initially specified equilibrium profile.

Equations (1) are solved numerically and initial perturbations develop until a saturated, quasistationary turbulence is reached. The impurities are then released into the turbulence and convected according to the evolving turbulent velocity field. The initial impurity density n_{imp} is chosen as a radially (coordinate x) localized Gaussian added onto an impurity background density. For some runs the impurity density was additionally localized along magnetic-field lines (coordinate s) to investigate the effect of parallel convective transport. The coupled system of bulk plasma turbulence and impurities is evolved until significant mixing of the impurities has been achieved and initial transient effects have decayed. For each parameter several runs are performed to increase the statistical significance of the results.

For passive fields in compressible fluid turbulence it is well known that the passive quantity reveals a much flatter fluctuation spectrum than the turbulent energy spectrum and that the passive scalar accumulates in the contracting regions of the turbulent flow [2]. The impurity density after some time not only exhibits strong gradients, but locally the initial value of the impurity density can be exceeded. To handle these effects within the given limited resolution the diffusive term in Eq. (3) was chosen as $\mu_{imp} = 5\mu_n$.

FIG. 1. Impurity distribution projected onto a poloidal cross section (radial dimension not to scale). White: high impurity density. Dark: low impurity density. Left: initial distribution, localized on the outboard midplane (at $s=0$). Right: after 25 time units corresponding to about 100 μs. Parallel transport is slow compared to radial transport. The inward pinch effect is clearly visible.

A prominent feature of the impurity behavior is the weak parallel convective transport compared to the radial turbulent transport, as parallel convection of impurities is due to the fluctuating parallel ion speed u which is small ($u \approx 0.01$) compared to radial velocities of order one. This is clearly observed in Fig. 1, which shows the impurity density. Here the complex flux tube geometry has been projected onto a geometrically poloidal cut. The projection roughly translates the parallel variation in s to a poloidal variation: $s=0$ is located at the outboard midplane, $s = \pm\pi/2$ at the upper resp. lower side, and finally $s = \pm\pi$ corresponds to the high-field side. The radial extend of the simulation domain has been stretched to allow better visualization. Initially the impurity density is localized at the outboard midplane ($s=0$). No significant parallel flow of the impurity density is observed, while significant radial mixing occurs. Parallel compressional effects are however visible and arrange for finite passive density gradients at the high-field side. Moreover, an inward pinch effect is clearly observed at the outboard midplane. Starting from an initial impurity distribution homogeneous along s, this pinching velocity is seen to shift the impurity density towards the torus axis (Fig. 2).

The flux Γ of the impurity ion species can in lowest order be expressed by the standard parameters used in modeling and in evaluation of transport experiments: a diffusion coefficient D and a velocity V, which is associated with a pinch effect,

$$\Gamma_y(s) = -D(s)\partial_x \langle n \rangle_y + V(s)\langle n \rangle_y. \tag{4}$$

The turbulence is radially homogeneous, so there is no radial dependence of D and V. Profiles $\langle \cdot \rangle_y$ are achieved by averaging over y, corresponding to averaging toroidally over the domain extend in the drift plane. From scatter plots of $\Gamma(r)/\langle n \rangle_y$ versus $\partial_x \langle \ln n \rangle_y$, values for $D(s)$ and $V(s)$ are obtained. The fitting procedure is carried out using a nonlinear

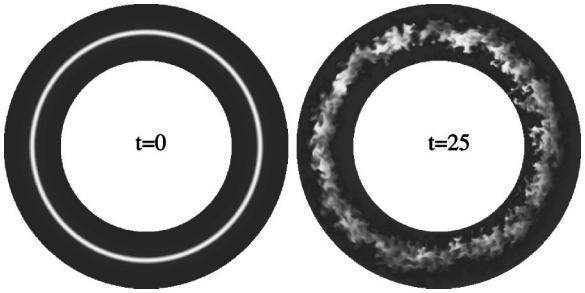

FIG. 2. Impurity distribution projected onto a poloidal cross section (radial dimension not to scale). Left: initial distribution. Right: after 25 time units. The inward pinch effect on the outboard midplane and outward convective transport on the high-field side (inboard midplane) is obvious.

least-squares Marquardt-Levenberg algorithm [12] as implemented within the plotting program GNUPLOT. To reduce the influence of numerical errors in the integration scheme on the transport estimate large gradients outside the range $[-0.1:0.1]$ are not considered for the fitting routine. Figure 3 shows a scatter plot with a fit. A comparison of the evolution of the impurity density profile with its presumed evolution using the values for D and V obtained from the above analysis is shown in Fig. 4. This shows that while the scatter plot has a significant amount of noise, the fitted values for D and V are reasonable parameters to represent the overall transport process.

The poloidal (coordinate s) dependence of D and V is rather strong and shown, with errors as obtained from the fitting routine, in Fig. 5. The effective convective velocity $V(s)$ changes sign and is at the high-field side directed outwards. This pinching velocity is due to curvature and can be consistently explained in the framework of turbulent equipartition (TEP) [1,13] as follows. In the absence of parallel convection, finite mass effects, and diffusion, Eq. (3) has the following approximate Lagrangian invariant:

$$L(s) = \ln n_{imp} + \omega_B \cos(s)x - \omega_B \sin(s)y. \qquad (5)$$

TEP assumes the spatial homogenization of L by the turbulence. As parallel transport is weak, each drift plane s

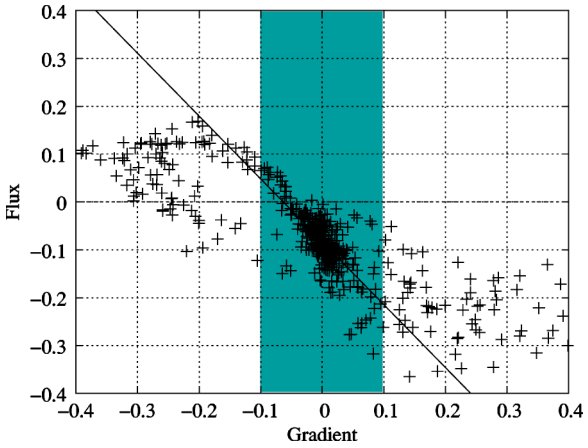

FIG. 3. Scatter plot (at high-field side) of flux vs gradient with linear fit. The gray area indicates gradients admissed for the fitting procedure.

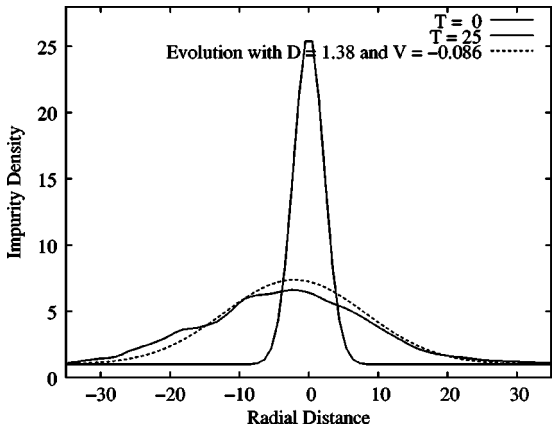

FIG. 4. Impurity density profile at the outboard midplane at $t=0$ and after 25 time units compared to the expected evolution of a Gaussian due to coefficients D and V obtained by the fitting procedure.

$=$const homogenizes independently. This leads to profiles $\langle L(s)\rangle_y = \text{const}(s)$. At the outboard midplane ($s=0$) the impurities are effectively convected radially inward leading to an impurity profile ($\langle \ln n_{imp}\rangle_y \propto \text{const} - \omega_B x$), while at the high-

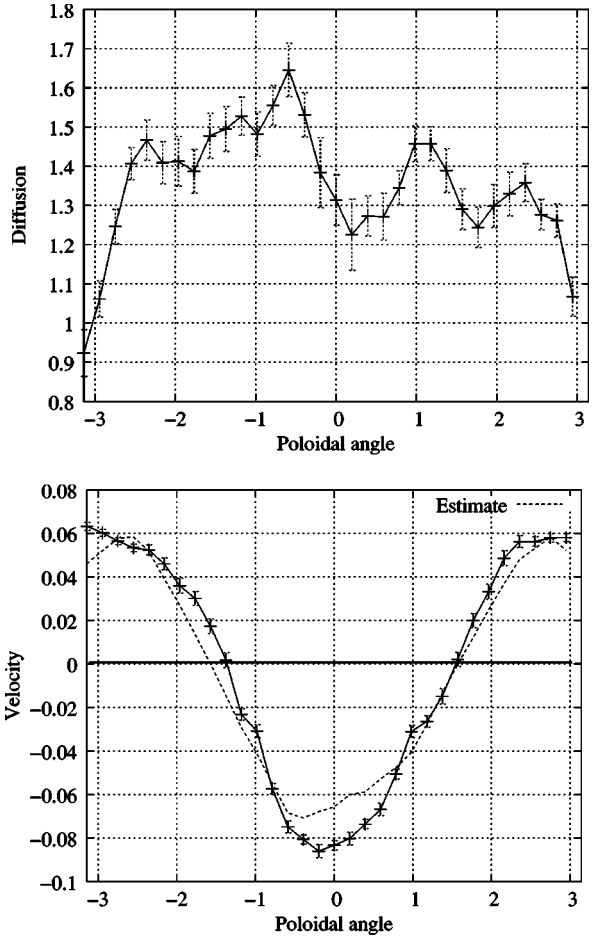

FIG. 5. Impurity diffusion D (top) and pinch velocity V (bottom) over poloidal position (s) with error bars. The pinch velocity is compared to $\omega_b * \cos(s) * D(s)$.

field side they are effectively convected outward ($\langle \ln n_{imp} \rangle_y \propto \text{const} + \omega_B x$). One should note that this effective inward or outward convection is not found as an average $E \times B$ velocity, but is mitigated by the effect of spatial homogenization of L under the action of the turbulence. The strength of the "pinch" effect is consequently proportional to the mixing properties of the turbulence and scales with the measured turbulent diffusion. We arrive at the following expression for the connection between pinch and diffusion:

$$V(s) = -\alpha \omega_B \cos(s) D(s). \tag{6}$$

Considering a stationary case with zero flux and combining Eqs. (4) and (5) we obtain $\alpha = 1$. The ballooning in the turbulence level causes the inward flow on the outboard midplane to be stronger than the effective outflow on the high-field side. Therefore, averaged over a flux surface and assuming poloidally constant impurity density, a net impurity inflow results. This net pinch is proportional to the diffusion coefficient D in agreement with experimental observations [14]. The proportionality constant will, however, depend on the amount of ballooning of the transport, which has been investigated f.x. in [7–9]. The level of ballooning of the transport increases with the transition from the drift regime to the magnetohydrodynamics (MHD) regime, as $\hat{\beta}$ increases to large values. Here, for small $hat\beta$ the ballooning of the transport is weak at about 70%.

Translated to dimensional values for typical large tokamak edge parameters we obtain $D(s) \propto 1.5 - 2.0\ \mathrm{m}^2/\mathrm{s}$ and $V(s) \propto (+60) - (-80)\ \mathrm{m/s}$ and a flux-surface averaged inward convection velocity of $\langle V \rangle = -0.4\ \mathrm{m/s}$. Locally at the outboard midplane values of $V(s=0)/D(s=0) \sim -40\ \mathrm{m}^{-1}$ are found, again in agreement with experimental values [3].

Due to the strong peaking of the impurity density, the poloidal dependence of the transport coefficients, and the slow parallel diffusion of the impurities the use of both a poloidally varying diffusion coefficient and effective convection velocity in transport codes to describe impurity density evolution, should lead to an improved overall description of turbulent impurity transport in toroidal magnetic confinement devices. The observed impurity pinch in the edge plasma region can be explained by turbulent equipartition resulting in a simple relation between diffusion and pinch velocity.

This work was supported by the Danish Center for Scientific Computing through Grants No. CPU-1101-08 and CPU-1002-17. Discussions with Jens Juul Rasmussen at Risø, and K.D. Zastrow and X. Garbet during a stay of the author at JET, are gratefully acknowledged.

[1] J. Nycander and V. V. Yan'kov, Phys. Plasmas **2**, 2874 (1995).
[2] G. Falkovich, K. Gawdzki, and M. Vergassola, Rev. Mod. Phys. **73**, 913 (2001).
[3] R. Dux, Fusion Sci. Technol. **44**, 708 (2003).
[4] M. E. Puiatti *et al.*, Plasma Phys. Controlled Fusion **45**, 2011 (2003).
[5] K. D. Zastrow, Nucl. Fusion **39**, 1891 (1999).
[6] P. H. Rutherford, Phys. Fluids **17**, 1782 (1974).
[7] B. D. Scott, Plasma Phys. Controlled Fusion **39**, 471 (1997).
[8] B. D. Scott, Plasma Phys. Controlled Fusion **39**, 1635 (1997).
[9] V. Naulin, Phys. Plasmas **10**, 4016 (2003).
[10] B. D. Scott, Phys. Plasmas **8**, 447 (2001).
[11] S. I. Braginskii, in *Reviews of Plasma Physics*, edited by M. A. Leontovich (Consultants Bureau, New York, 1965).
[12] D. Marquardt, J. Soc. Ind. Appl. Math. **11**, 431 (1963).
[13] V. Naulin, J. Nycander, and J. Juul Rasmussen, Phys. Rev. Lett. **81**, 4148 (1998).
[14] M. E. Perry *et al.*, Nucl. Fusion **31**, 1859 (1991).